Second Harmonic Scattering of Redox Exfoliated Two-Dimensional Transition Metal Dichalcogenides

Melissa Maldonado, Anderson Amaral, Zacharie Behel, Estelle Salmon, Cid B de Araújo, Anderson S L Gomes, Ali M Jawaid, Allyson J Ritter, Richard A Vaia, Christian Jonin, et al.

Second Harmonic Scattering of Redox Exfoliated Two-Dimensional Transition Metal Dichalcogenides

Melissa Maldonado,[a] Anderson Amaral,[a] Zacharie Behel,[b] Estelle Salmon,[b] Cid B. de Araújo,[a] Anderson S.L. Gomes,[a] Ali M. Jawaid,[c] Allyson J. Ritter,[c] Richard A. Vaia,[c] Christian Jonin,[b] Pierre-François Brevet[b]*

[a]Departamento de Física, Universidade Federal de Pernambuco, Av. Prof. Moraes Rego, 1235, Cidade Universitária, Recife, PE 50670-901, Brazil E-mail: anderson@df.ufpe.br

[b]Institut Lumière Matière, Université de Lyon, UMR 5306 CNRS and Université Claude Bernard Lyon 1, 69622 Cedex, Villeurbanne, France

[c]Materials and Manufacturing Directorate, Air Force Research Laboratories, 45433, Ohio, United States.

AUTHOR INFORMATION

Corresponding Author

*Pierre-François Brevet, pfbrevet@univ-lyon1.fr

ABSTRACT.

We report the second harmonic scattering experiments from acetonitrile liquid suspensions of two-dimensional metal dichalcogenide nanoflakes, the semiconducting MoS_2 and WS_2, the metallic NbS_2 and the semi-metallic $ZrTe_2$. Because the study is directly performed in the liquid phase, no symmetry breaking can be attributed to a supporting substrate as it is often the case in the investigation of the second harmonic generation efficiency for these materials. A comparative look of the origin of the nonlinear response using polarization analysis of the hyper Rayleigh scattering intensity is performed. Retardation is clearly exhibited by all nanoflakes considering their average dimensions. This is attributed to the non-negligible role played by the edges in all cases.

KEYWORDS. Second Harmonic Scattering, Femtosecond Regime, Layered Transition Metal Dichalcogenides, Two-Dimensional Materials

INTRODUCTION

Two-dimensional (2D) materials have been studied over the last several years, and among them layered transition metal dichalcogenides (LTMDs) have accomplished outstanding performances,[1,2] leading to a diversity of applications.[3-5] In all-optical applications for example, their second, third and even higher order optical nonlinearities are of great interest. Nonlinear optical (NLO) properties of 2D LTMDs have thus been studied and the corresponding nonlinear susceptibilities have been determined. They are found to be higher than their bulk material counterpart, as reviewed by Autere et al.[6] Although most of the work carried out so far exploits the semiconducting 2D LTMDs family, particularly the MoX_2 and WX_2 (X = S, Se) families[1-6] other 2D LTMDs have been synthesized by different methods, such as modified redox exfoliation,[7] whose detailed synthesis mechanism has been recently modeled,[8] leading to metallic and semi-metallic 2D layered LTMDs besides the semiconducting ones.[9] The second order NLO properties of these materials have been well investigated for the above-mentioned semiconducting materials using coherent second harmonic generation as the method of choice.[6,10-18] As a notable exception, Forcherio et al. employed hyper Rayleigh scattering (HRS) to characterize the second-order nonlinear susceptibility $\chi^{(2)}$ for liquid exfoliated semiconducting WS_2 monolayers using 1ns duration pulses at 1064 nm.[19,20] HRS provides indeed a direct measurement of $\chi^{(2)}$ once the volume is known that can be analyzed in light of other parameters like point group symmetries. HRS is a method originally employed in molecular liquid solutions[21] to determine the orientation-averaged nonlinear second order efficiency of molecules by correlating their scattered SHG intensity with their molecular concentration.[22] Rodriguez and co-workers[23] and Le Dantec and co-workers[24] have exploited the method to obtain the second order nonlinear properties of sub-wavelength nanoparticles with appropriate conversion from per-nanoparticle to their bulk material counterpart. Since then, HRS has been employed to characterize second order

nonlinearities of nanomaterials, and in this work, we report its use in its polarization resolved modality for four different 2D LTMDs materials, namely the semiconducting MoS_2 and WS_2, metallic NbS_2 and semi-metallic $ZrTe_2$, prepared by the redox exfoliation method.[7,8] The nanoscale size of the 2D material flakes invites indeed to directly investigate hyperpolarizabilities rather than macroscopic quantities. The nonlinear response of all four materials in solution using this polarization modality was determined using 800 nm, 140 fs pulse duration at 80 MHz input repetition rate and we employed as the external reference the acetonitrile solvent.[25]

EXPERIMENTAL METHODS

Synthesis: The 2D LTMDs materials reported here were synthesized and morphologically characterized by Jawaid et al..[7,8] Samples of MoS_2, WS_2, NbS_2 and $ZrTe_2$ nanoflakes were employed in this work. Although a thorough description of the preparation method is described in Refs.7 and 8, a short summary is given here. The redox exfoliation of metal-dichalcogenides of general MX_2 formula was basically carried out by sequential surface oxidation and reduction reaction with a weak organic hydroperoxide and an inorganic reducing agent. The synthesis started with the suspension of bulk TMDs powder in acetonitrile solvent followed by weak oxidation treatment resulting in the formation of peroxometalate precursors and TMD sedimentation. The subsequent addition of a reducing agent in the solution triggered the formation of anionic polyoxometalates (POMs). Such POMs were adsorbed to the basal surface of TMDs, thereby creating a Coulombic repulsion force to facilitate few-layer exfoliation.

Surface oxidation: Prior to synthesizing LTMDs, the round-bottom flasks were cleaned and an inert environment was maintained in order to minimize side reactions. Exemplifying with

MoS_2, initially, bulk powder of 0.625 mmol suspended in 5 mL of acetonitrile (CH3CN, ACN) was added into the flask and stirred at 0 ºC over an ice bath for 30 min. After reaching thermal equilibrium, a mixture of 3 mmol of cumene hydroperoxide (80 % CHP) and 5 mL of acetonitrile was introduced dropwise into the previously prepared MoS_2 suspension for every 15 min under constant stirring at 0 ºC. After the complete addition of CHP, the bath solution was stirred at 25 ºC for 24 hours. Similar process recipes were followed for the surface oxidation of WS_2, NbS_2 and $ZrTe_2$ with appropriate bath temperatures.[7,8]

Exfoliation: After the settlement of the MoS_2 powder at the flask bottom, the oxidized solution volume was reduced to 4 mL and stirred at 0 ºC for 30 min. After reaching equilibrium, 50 μL aqueous solution of 100 mM $NaBH_4$ was introduced into the above oxidized solution and kept under constant stirring for 1 h. The process was repeated few times to increase the solution volume. The solution was stirred at room temperature for 24 h and allowed to settle down the un-exfoliated flakes. Later, the supernatant was isolated, centrifuged at 10,000 rpm for 15 min to sediment the exfoliated flakes. Finally, the exfoliated monolayer MoS_2 flakes were obtained with successive sedimentation and redispersion in fresh anhydrous acetonitrile. Similar process recipes were followed for the exfoliation of WS_2, NbS_2 and $ZrTe_2$ LTMDs. All the exfoliated monolayer TMD samples were isolated for the morphological and structural characterization by employing SEM, AFM, TEM and XRD, whose results are shown in Refs. 7 and 8. The nanoflakes physical dimensions are shown in Tables 1, together with the second harmonic scattering (SHS) results.

AFM measurements were made to obtain sample thicknesses. Dilute solutions of LTMD ($\sim 10^{-8}$ M) were drop-cast onto Si wafers and dried in a vacuum oven (100^{o}C. 1 hour) to ensure removal of solvent. The sample was then transferred to a Bruker Dimension Icon and

particles were imaged in non-contact tapping mode. The resultant micrographs were analyzed for particle height distributions. Due to the processing history of liquid phase exfoliated 2D materials, AFM measurements typically over-estimate actual heights due to tip-surface interactions and surface adsorbed species interacting with the cantilever tip electronically.[26,27] The true monolayer height is typically not observed, and alternative metrics can be used to calibrate the observed height to the actual height. One such method, utilized in this manuscript, derives the observed monolayer height via analyzing the quantized height in a step-wise fashion.[28]

Nonlinear optics. The experimental setup for the SHS measurements has been reported in earlier works[29] and references therein. Briefly, a Ti:Sapphire laser (Coherent, Chamaleon Ultra), operating at 800 nm and delivering pulses of 140 fs duration at 80 MHz repetition rate was used. The laser beam was sent through a waveplate and Glan polarizer for controlling the power. After that, a high pass filter was used to eliminate residual pump radiation. The beam was focused by a 10X objective (Thorlabs, LMH-10x-532) and a cuvette containing the sample solution was put in the focal point. The SHS emission was collected at right angle with respect to the incident beam. A low pass filter was put at the entrance of the detector, a monochromator in front of a photomultiplier tube, for collecting only the photons with frequency 2ω. The monochromator allowed the spectrally resolved measurement of the scattered light from 390 nm to 410 nm to observe the SHS signal. It also allowed the removal of any unwanted stray light or sample luminescence. For the polarization resolved measurements, a rotating half-wave plate was introduced before the cell and a half-wave plate plus a Glan polarizer adapted to 400 nm in front of the monochromator entrance. This waveplate was fixed at two positions: 0º for vertical polarization (noted V) and 90º for the horizontal polarization (noted H) of the SHS signal with respect to the laboratory frame. All

measurements consisted in 10 seconds integration time. A single long integration time was preferred for larger counts detected as opposed to shorter integration times repeated. However, linearity of the total count with time was checked before hand.

RESULTS AND DISCUSSION

Physical properties. From the collected data, the samples are typically ~60% monolayers, based on AFM height measurements. The exfoliated semiconducting MoS_2 and WS_2, and the exfoliated metallic NbS_2 were of 2H symmetry, as observed by TEM and Raman spectroscopy.[7,8,30] We note that in ref. 29, besides the Raman and other morphological characterizations, the third order optical nonlinearities of exfoliated 2D LTMD metallic NbS_2 was reported. On the other hand, the semi-metallic exfoliated 2D LTMDs $ZrTe_2$ is in the 1T phase symmetry, and since the literature on its Raman spectra is scarce, we show in Figure 1 the data for the exfoliated sample employed in this work, as well as for a bulk powder sample. The peaks identified in bulk samples correspond to the E_{2g} (c.a. 116 cm^{-1}) and A_{1g} (c.a. 137 cm^{-1}) modes of the 1T phase.[31]

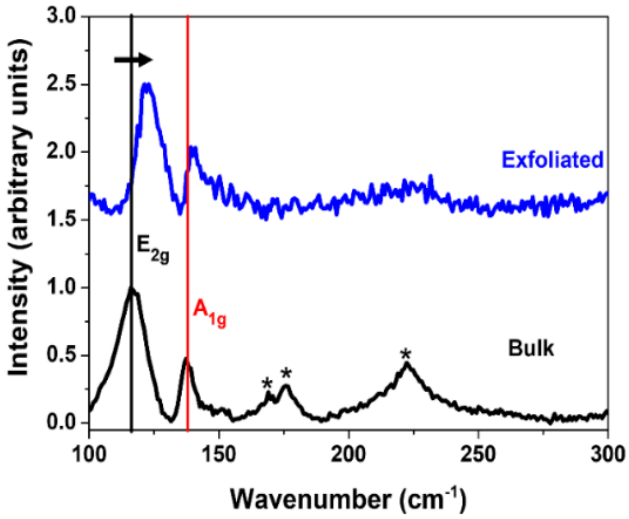

Figure 1: Raman spectra of ZrTe2 at 298K (room temperature). Exfoliated and bulk materials are shown for comparison. A blue shift is observed of the presumed E_{2g} and A_{1g} modes.

Additional features in the bulk sample corresponding to monoclinic ZrO_2 are observed (indicated by asterisks).[32] Upon exfoliation, the E_{2g} mode blue-shifts by approximately 7 cm^{-1}, as observed for other layered systems,[33,34] indicating the absence of phase change. The absence of ZrO_2 features indicates that the exfoliation process does not lead to significant oxidation of the $ZrTe_2$ material provided with the anhydrous sample preparation.

Linear optical properties. Figure 2 shows the linear extinction for all samples in acetonitrile solution. The spectra for MoS_2 and WS_2 show the characteristic peaks assigned to the A-exciton transitions (2H-MX2).[7] On the other hand, the metallic NbS_2 and semi-metallic $ZrTe_2$ have smooth (i.e. no salient absorption peaks) spectra, characteristic of metallic materials.

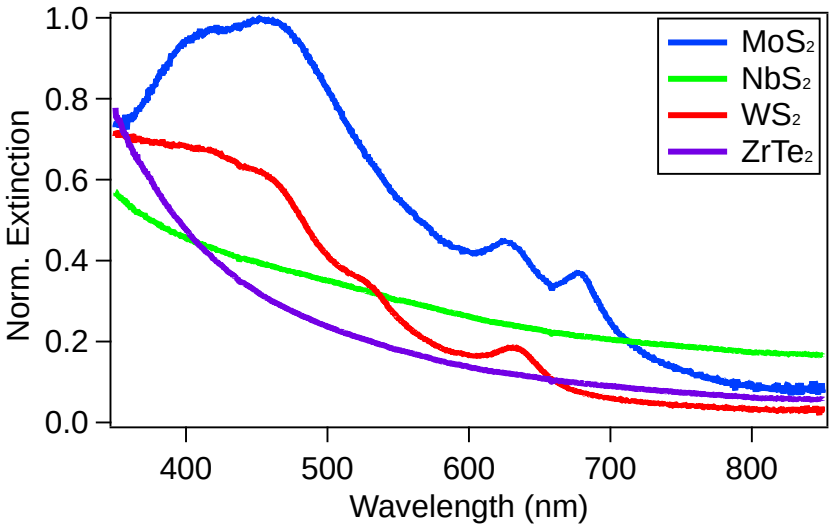

Figure 2: Normalized UV-visible extinction spectra for the four samples. (blue) MoS_2, (green) NbS_2, (red) WS_2 and (purple) $ZrTe_2$.

Polarization Resolved SHS. Because the exact concentration of the samples could not be obtained with sufficient precision, the first hyperpolarizability of these compounds is not reported. Rather, we have focused on the origin of the nonlinear response using polarization

resolved measurements where, as a function of the fundamental beam angle of polarization, the resulting SHS intensity can be written as:[39]

$$I_{HRS}^{\Gamma}(\gamma) = a^{\Gamma}\cos^4\gamma + b^{\Gamma}\sin^2\gamma\cos^2\gamma + c^{\Gamma}\sin^4\gamma \quad (1)$$

The a^{Γ}, b^{Γ} and c^{Γ} intensity coefficients are all obtained from the adjustment of the experimental data given in Figure 3 to provide the depolarization coefficient D^{V} and the retardation coefficients ζ^{Γ} where Γ refers to vertical (V) or horizontal (H) polarizations with respect to the plane of scattering. The depolarization coefficient is given by:

$$D^{\mathrm{V}} = c^{\mathrm{V}}/a^{\mathrm{V}} \quad (2)$$

whereas the retardation coefficients are:

$$\zeta^{V} = (b^{V} - a^{\mathrm{V}} - c^{\mathrm{V}})/b^{\mathrm{V}} \quad (3a)$$

$$\zeta^{H} = (a^{H} - c^{\mathrm{H}})/(a^{H} + c^{\mathrm{H}}) \quad (3b)$$

All parameters extracted from the polarization SHS experiments given in Figure 3 are compiled in Table 1. All plots exhibit a two-lobe pattern for the vertically polarized SHS intensity with a minor deviation not exceeding 20% from the un-retarded response for which $\zeta^{V} = \zeta^{H} = 0$. For the horizontally polarized SHS intensity along the 90° angle of polarization direction, flattened circular plots are observed in all cases.

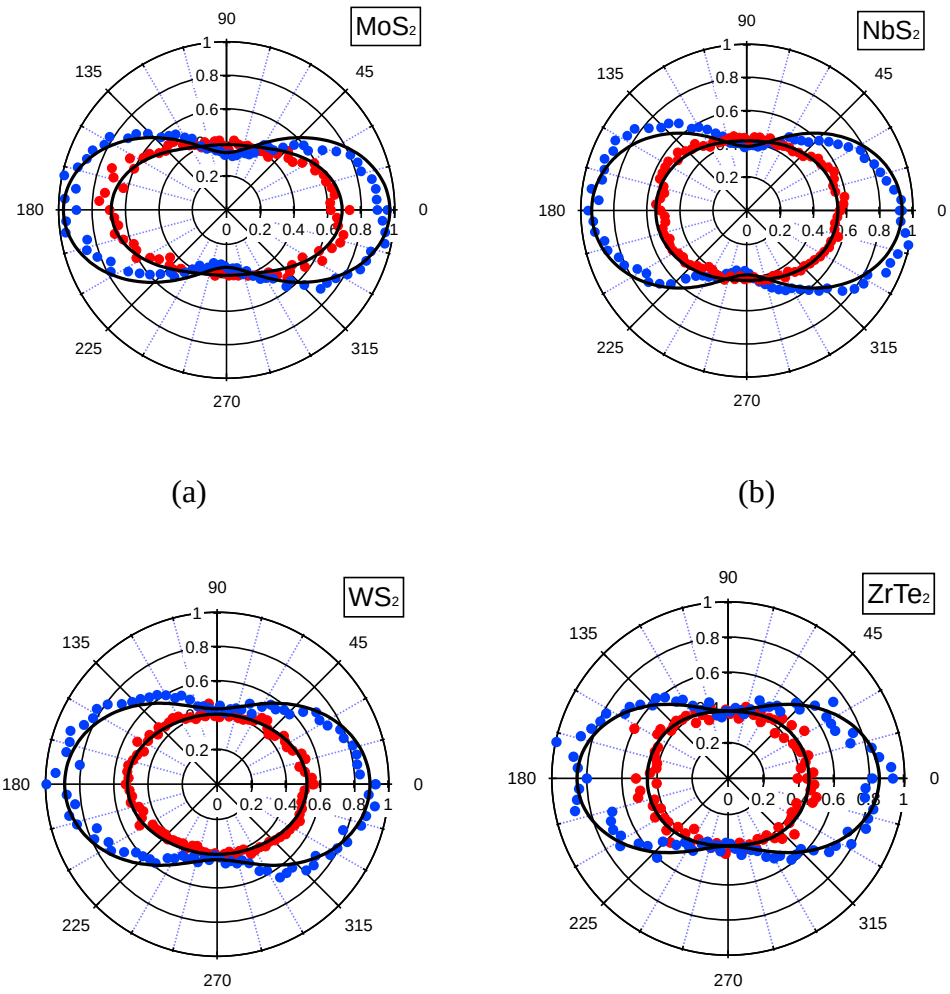

(a) (b)

(c) (d)

Figure 3: Polarization resolved plots of the SHS intensity for (a) MoS_2, (b) NbS_2, (c) WS_2 and (d) $ZrTe_2$. Blue circles are V polarized harmonic intensity and red circles are H polarized harmonic intensity. The black lines are fits using Eq. (1).

The depolarization ratio exhibited by all samples largely deviates from the expected theoretical ratio of 2/3 expected for a flat octupolar symmetry nonlinearity. This underlines the possible role of the nanoflake edges in contributing to the total nonlinearity of the system besides the non-centrosymmetric volume contribution. Nevertheless, in liquid suspensions, the flexibility of the nanoflakes with nanoscale dimensions may also play some role in breaking the true octupolar symmetry due to folding or wrinkling. All these features must be

accounted for in order to fully explain in a quantitative manner the present experimental results and the deviation to the standard equalities between hyperpolarizability tensor elements as expected for perfect geometries. Retardation, as seen from the non-vanishing retardation parameters values remains rather weak, this feature being explained by the strong volume origin of the nonlinearity due to the non-centrosymmetry of the crystal lattice structure, either inherent or broken, as in $ZrTe_2$.

Table 1: Parameters determined from polarizations plots.

Sample	**Avg. lateral extension (nm, TEM)**	ζ_V	ζ_H	D^V
MoS_2	84	-0.18	-0.22	0.35
WS_2	325 ± 75	-0.05	-0.06	0.49
NbS_2	121	-0.03	0.01	0.41
$ZrTe_2$	150	-0.12	0.04	0.45
Acetonitrile		-0.09	0.02	0.28

It is seen from Table 1 that MoS_2 presents the largest retarded effects. One possible reason for this behavior may stem from the edges contribution sensibly the largest of all samples as compared to the volume contribution. This point may be further underlined by the weaker depolarization ratio as well.

Modeling of the SHS response. In order to further describe the SHS intensities collected from these two-dimensional nanoflakes, a model based on the use of a distribution of local

non-polarisable nonlinear dipoles was devised. A central non-linear dipole was used to describe the volume contribution from the nanoflake, the materials presenting a non-centrosymmetric crystal lattice structure. The nanoflake edges were then modelled with distributed nonlinear dipoles either oriented normal to the edges, see Figure 4(a, b) or along the edges, see Figure 4(c, d). In the case of an orientation along the edges, the resulting polarization plot is dominated by a dipolar pattern for the V-polarized SHS intensity as a function of the input polarization angle. This pattern is associated with a vanishing ζ^V value. The H-polarization pattern is in this case rather circular or slightly elliptical and is associated also with a vanishing ζ^H value. On the opposite, it appears that in the case of a response normal to the edge, the V-polarized SHS intensity develops a quadrupolar pattern associated with a larger ζ^V value and a H-polarized SHS intensity pattern corresponding a larger ζ^H value as well.

These results suggest therefore that, besides the dominating dipolar volume response of MoS_2 due to the non-centrosymmetry of the crystal structure, a non-vanishing edge response is also present. This is even more evident for the centro-symmetric $ZrTe_2$ exhibiting similarly a large retardation parameter because the volume contribution does not exist apart from centrosymmetry breaking due to local environment and possible floppiness. However, it is difficult at this stage to identify one model only as many parameters must be considered, in particular the ratio between the edges and the volume hyperpolarizabilities. In any case, for WS_2 and NbS_2 that exhibit a dominating dipolar volume response, the dominating contribution stems from the non-centrosymmetric volume. On a final note, we add that the flattening observed for horizontally polarized polar plots stems essentially from the excited modes of the multipolar expansion of the SHS intensity response.

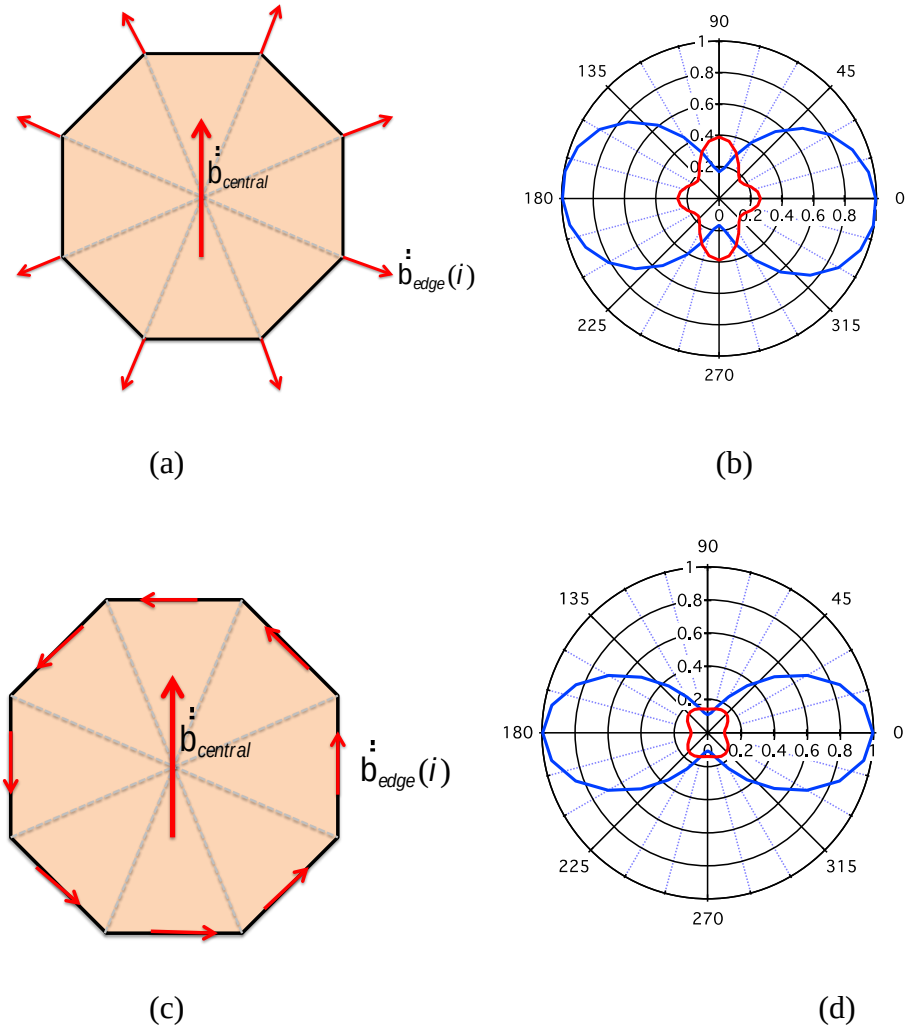

Figure 4: Model of the non-centrosymmetric two-dimensional material nanoflakes. (a) Model of a radial edge nonlinear dipoles distribution, (b) corresponding polarization resolved plot of the SHS intensity, (blue) vertically polarized intensity, (red) horizontally polarized intensity, (c) Model of a tangential edge nonlinear dipoles distribution, (d) corresponding polarization resolved plot of the SHS intensity, (blue) vertically polarized intensity, (red) horizontally polarized intensity.

CONCLUSIONS

A detailed comparative SHS study for four two-dimensional metal dichalcogenide materials, namely MoS_2, WS_2, NbS_2 and $ZrTe_2$, produced by redox exfoliation is performed. Retardation is rather weak in all materials as a result of the non-centrosymmetry of the crystal lattice

structure, even in the case of $ZrTe_2$ where the volume non centrosymmetry may stem from the local environment and possible floppiness. The experimental data also points to a non-negligible contribution from the nanoflake edges, particularly in the case of MoS_2. These results provide a direct comparison of these four two-dimensional dichalcogenide materials in absence of substrate and should provide a benchmark for future theoretical approaches to these systems.

Conflicts of interest

There are no conflicts to declare.

ACKNOWLEDGEMENTS

AMJ, AJR, and RAV thank AFOSR and the Air Force Research Laboratory Materials and Manufacturing Directorate for financial support. MM, AA, CBdA and ASLG also thank the financial support from CNPq, FACEPE and CAPES. ChJ and PFB acknowledge financial support from the French Agence Nationale pour la Recherche under grant number CE24-RACINE-2017.

REFERENCES

(1) Wei, Z.; Li, B.; Xia, C.; Cui, Y.; He, J.; Xia, J.B.; Li, J. Various structures of 2D transition-metal dichalcogenides and their applications. *Small Methods* **2018**, 2, 1800094.

(2) Choi, W.; Choudhary, N.; Han, G.H.; Park, J.; Akinwande, D.; Lee, Y.H. Recent development of two-dimensional transition metal dichalcogenides and their applications. *Mater. Today* **2017**, 20, 116.

(3) Han, S.A.; Bhatia, R.; Kim, S.W. Synthesis, properties and potential applications of two-dimensional transition metal dichalcogenides. *Nano Convergence* **2015**, 2, 17.

(4) Huo, N.; Yang, Y.; Li, J. Optoelectronics based on 2D TMDs and heterostructures. *J. Semicond.* **2017**, 38, 031002.

(5) Kurapati, R.; Kostarelos, K.; Prato, M.; Bianco, A. Biomedical uses for 2D materials beyond graphene: current advances and challenges ahead. *Adv. Mater.* **2016**, 28, 6052.

(6) Autere, A.; Jussila, H.; Dai, Y.; Wang, Y.; Lipsanen, H.; Sun, Z. Nonlinear optics with 2D layered materials. *Adv. Mater.* **2018**, 30, 1705963.

(7) Jawaid, A.M.; Che, J.; Drummy, L. F.; Bultman, J.; Waite, A.; Hsiao, M.S.; Vaia, R.A. Redox exfoliation of layered transition metal dichalcogenides. *ACS Nano* **2017**, 11, 635 and references therein.

(8) Jawaid, A.M.; Ritter, A.J.; Vaia, R.A. Mechanism for liquid phase exfoliation of MoS_2. *Chem. Mater*. **2020**, 32, 6550.

(9) Yan, C.; Gong, C.; Wangyang, P.; Chu, J.; Hu, K.; Li, C.; Wang, X.; Du, X.; Zhai, T.; Li, Y.; Xiong, J. 2D group IVB transition metal dichalcogenides. *Adv. Func. Mater.* **2018**, 28, 1803305.

(10) Wang, Y.; Xiao, J.; Yang, S.; Wang, Y.; Xiang, Z. Second harmonic generation spectroscopy on two-dimensional materials. *Opt. Mater. Express* **2019**, 9, 1136.

(11) Kumar, N.; Najmaei, S.; Cui, Q.; Ceballos, F.; Ajayan, P.M.; Lou, J.; Zhao, H. Second harmonic microscopy of monolayer MoS_2. *Phys. Rev. B* **2013**, 87, 161403.

(12) Hsu, W.T.; Zhao, S.A.; Li, L.J.; Chen, C.-H.; Chiu, M.-H.; Chang, P.-S.; Chou, Y.-C.; Chang, W.-H. Second harmonic generation from artificially stacked transition metal dichalcogenide twisted bilayers. *ACS Nano* **2014**, 8, 2951.

(13) Ribeiro-Soares, J.; Janisch, C.; Liu, Z.; Eliás, A.L.; Dresselhaus, M.S.; Terrones, M.; Cançado, L.G.; Jorio, A. Second harmonic generation in WSe_2. *2D Mater.* **2015**, 2, 045015.

(14) Rosa, H.G.; Wei, H.Y.; Verzhbitskiy, I.; Rodrigues, M.J.F.L.; Taniguchi, T.; Watanabe, K.; Eda, G.; Pereira, V.M.; Gomes, J.C.V. Characterization of the second- and third harmonic optical susceptibilities of atomically thin tungsten diselenide. *Sci. Rep.* **2018**, 8, 10035.

(15) Mennel, L.; Paur, M.; Mueller, T. Nonlinear optics in 2D materials. *APL Photonics* **2019**, 4, 034404.

(16) Wei, Y.; Xu, X.; Wang, S.; Li, W.; Jiang, Y. Second harmonic generation in Janus MoSSe a monolayer and stacked bulk with vertical asymmetry. *Phys. Chem. Chem. Phys*. **2019**, 21, 21022.

(17) Li, Y.; Rao, Y.; Mak, K.F.; You, Y.; Wang, S.; Dean, C.R.; Heinz, T.F. Probing Symmetry Properties of Few-Layer MoS_2 and h-BN by Optical Second-Harmonic Generation. *Nano Lett.* **2013**, 13, 3329.

(18) Steves, K.F.; Wang, Y.; Briggs, N.; Zhao, T.; El-Sherif, H.; Bersch, B.M.; Subramanian, S.; Dong, C.; Bowen, T.; De La Fuente Duran, A. et al. Unexpected Near-Infrared to Visible Nonlinear Optical Properties from 2-D Polar Metals. *Nano Lett.* **2020**, 20, 8312.

(19) Forcherio, T.G.; Riporto, J.; Dunklin, R.J.; Mugnier, Y.; Le Dantec, R.; Bonacina, L.; Roper, D.K. Nonlinear optical susceptibility of two-dimensional WS_2 measured by hyper Rayleigh scattering. *Opt. Lett.* **2017**, 43, 2400. Erratum, *Opt. Lett.* **2018**, 43, 2400.

(20) da Silva-Neto, M.L.; Barbosa-Silva, R.; de Araujo, C.B.; de Matos, C.J.S.; Jawaid, A.M.; Ritter, A.J.; Vaia, R.A.; Gomes A.S.L. Hyper–Rayleigh scattering in 2D redox exfoliated semi-metallic ZrTe2 transition metaldichalcogenide. *Phys. Chem. Chem. Phys*. **2020**, 22, 27845.

(21) Clays, K.; Persoons, A. Hyper Rayleigh scattering in solution. *Phys. Rev. Lett*. **1991**, 66, 2980.

(22) Hubbard, S.F.; Petschek R.G.; Singer K.D. Spectral content and dispersion of hyper-Rayleigh scattering. *Opt. Lett*. **1996**, 21, 1774.

(23) Rodriguez, E.V.; de Araújo, C.B.; Brito-Silva, A.M.; Ivanenko, V.I.; Lipovskii, A.A. Hyper-Rayleigh scattering from $BaTiO_3$ and $PbTiO_3$ nanocrystals. *Chem. Phys. Lett*. **2009**, 467, 335.

(24) Le Dantec, R.; Mugnier, Y.; Djanta, G.; Bonacina, L.; Extermann, J.; Badie, L.; Joulaud, C.; Germann, M.; Rytz, D.; Wolf, J.P. et al. Ensemble and individual characterization of the nonlinear optical properties of ZnO and $BaTiO_3$ nanocrystals. *J. Phys. Chem. C* **2011**, 115, 15140.

(25) Pauley, M.A.; Guan, H.W.; Wang, C.H.; Jen, A.K.Y. Determination of first hyperpolarizability of nonlinear optical chromophores by second harmonic scattering using an external reference. *J. Chem. Phys.* **1996**, 104, 7821.

(26) Shearer, C.J.; Slattery, A.D.; Stapleton, A.J.; Shapter, J.G.; Gibson, C.T. Accurate thickness measurement of graphene. *Nanotechnol.* **2016**, 27, 125704.

(27) Vallés, C.; Drummond, C.; Saadaoui, H.; Furtado, C.A.; He, M.; Roubeau, O.; Ortolani, L.; Monthioux, M. ; Pénicaud, A. Solutions of Negatively Charged Graphene Sheets and Ribbons. *J. Am. Chem. Soc.* **2008**, 130, 15802.

(28) Backes, C.; Smith, R.J.; McEvoy, N.; Berner, N.C.; McCloskey, D.; Nerl, H.C.; O'Neill, A.; King, P.J.; Higgins, T.; Hanlon, D. et al. Edge and confinement effects allow *in situ* measurement of size and thickness of liquid-exfoliated nanosheets. *Nat. Commun.* **2014,** 5, 4576.

(29) Butet, J.; Maurice, A.; Bergmann, E.; Bachelier, G.; Russier-Antoine, I.; Ray, C.; Bonhomme, O.; Jonin, C.; Benichou, E.; Brevet, P.F. Second harmonic generation with metallic nanoparticles in Metal nanostructures for photonics, Eds Kassab, L.R.P. and de Araújo, C.B., Elsevier, Amsterdam, 2019.

(30) Maldonado, M.; da Silva Neto, M.L.; Vianna, P.G.; Ribeiro, H.B.; Gordo, V.O.; Carvalho, I.C.S; Menezes, L. de S.; de Araújo, C.B.; de Matos, C.J.S.; Seixas, L. et al. Femtosecond nonlinear optical properties of 2D metallic NbS_2 in the near infra-red. *J. Phys. Chem. C* **2020**, 124, 15425.

(31) Hangyo, H.M.; Nakashima, S.-I.; Mitsuishi, A. Raman spectroscopic studies of MX_2-type layered compounds. *Ferroelectrics* **1983**, 52, 151.

(32) Eder, D.; Kramer, R. The stoichiometry of hydrogen reduced zirconia and its influence on catalytic activity. Part 1: Volumetric and conductivity studies. *Phys. Chem. Chem. Phys*. **2002**, 4, 795.

(33) Li, H.; Zhang, Q.; Yap, C.C.R.; Tay, B.K.; Edwin, T.H.T.; Olivier, A.; Baillargeat, D. From bulk to monolayer MoS_2 : Evolution of Raman scattering. *Adv. Func. Mater.* **2012**, 22, 1385.

(34) Wang, F.; Kinloch, I.A.; Wolverson, D.; Tenne, R.; Zak, A.; O'Connell, E.; Bangert, U.; Young, R.J. Strain-induced phonon shifts in tungsten disulfide nanoplatelets and nanotubes. *2D Mater*. **2016**, 4, 015007.

(39) Nappa, J.; Revillod, G.; Russier-Antoine, I.; Benichou, E.; Jonin, C.; Brevet, P.F. Electric dipole origin of the second harmonic generation from small metallic particles. *Phys. Rev. B* **2005**, 71, 165407.

GRAPHICAL ABSTRACT